

Article

Pd-Nanoparticle-Decorated Multilayered MoS₂ Sheets for Highly Sensitive Hydrogen Sensing

Shuja Bashir Malik^{1,2}, Fatima Ezahra Annanouch^{1,2,*}  and Eduard Llobet^{1,2} 

¹ Departament d'Enginyeria Electronica, Universitat Rovira i Virgili, MINOS, Paisos Catalans 26, 43007 Tarragona, Spain; shujabashir.malik@urv.cat (S.B.M.); eduard.llobet@urv.cat (E.L.)

² Institut Universitari de Recerca en Sostenibilitat, Canvi Climàtic i Transició Energètica, Universitat Rovira i Virgili, Joanot Martorell 15, 43480 Vila-seca, Spain

* Correspondence: fatimaezahra.annanouch@urv.cat

Abstract: In this work, efficient hydrogen gas sensors based on multilayered p-type bare MoS₂ and Pd-decorated MoS₂ were fabricated. MoS₂ was deposited onto alumina transducers using an airbrushing technique to be used as a sensing material. Aerosol-assisted chemical vapor deposition (AACVD) was used to decorate layered MoS₂ with Pd nanoparticles at 250 °C. The bare and Pd-decorated MoS₂ was characterized using field emission scanning electron microscopy (FESEM), high-resolution transmission electron microscopy (HR-TEM), X-ray diffraction (XRD), and Raman spectroscopy. The characterization results reveal the multilayered crystalline structure of MoS₂ with successful Pd decoration. The size of the Pd nanoparticles ranges from 15 nm to 23 nm. Gas sensing studies reveal that a maximum response of 55% is achieved for Pd-decorated MoS₂ operated at 150 °C to 100 ppm of H₂, which is clearly below the explosive limit (4%) in air. The higher sensitivity due to Pd nanoparticle decoration was owed to a spillover effect. This study reveals that the sensitivity of the sensors is highly dependent on the amount of Pd decoration. Moreover, sensor responses increase slightly when exposed to 50% relative humidity (RH at 25 °C).

Keywords: gas sensor; spillover; nanoparticles; TMDs; AACVD; decoration



Citation: Malik, S.B.; Annanouch, F.E.; Llobet, E. Pd-Nanoparticle-Decorated Multilayered MoS₂ Sheets for Highly Sensitive Hydrogen Sensing. *Chemosensors* **2023**, *11*, 550. <https://doi.org/10.3390/chemosensors11110550>

Academic Editor: Simonetta Capone

Received: 6 September 2023

Revised: 20 October 2023

Accepted: 24 October 2023

Published: 26 October 2023



Copyright: © 2023 by the authors. Licensee MDPI, Basel, Switzerland. This article is an open access article distributed under the terms and conditions of the Creative Commons Attribution (CC BY) license (<https://creativecommons.org/licenses/by/4.0/>).

1. Introduction

The ever-increasing demand for sustainable and clean energy sources has put hydrogen (H₂) at the forefront as one of the most promising candidates for the next generation of energy. Due to the abundance of hydrogen in nature, it offers the potential in the future to replace fossil fuels as its combustion yields water; thus, it will [1] significantly reduce greenhouse gas emissions [2]. However, hydrogen is highly explosive and flammable (air mixtures at H₂ concentrations above 4%), which demands the utmost caution in its storage and handling [3]. Even a small leakage of hydrogen can pose a grave threat to safety. Therefore, the development of highly sensitive and selective hydrogen gas sensors with fast detection and recovery are of paramount importance to detect and mitigate potential hazards associated with hydrogen storage, transport, and leakage.

Metal oxide gas sensors (MOX) have been widely used for hydrogen sensing [4], but they suffer from several limitations like poor selectivity and a high working temperature (200–400 °C) [5–7]. This leads to an increase in the power consumption and, at the same time, reduces a sensor's lifetime by inducing changes in the material morphology [8]. Moreover, with hydrogen being extremely flammable, sensors working at high temperatures could be potentially dangerous [9], requiring necessary remedies to mitigate damage. Recently, the scientific community has turned its attention towards two-dimensional materials (2D) to overcome the shortcomings of MOX sensors. Indeed, 2D materials have garnered tremendous attention due to their unique electronic and remarkable sensing properties [10,11]. Among 2D materials, on the one hand, graphene has demonstrated outstanding sensing capabilities for toxic gases like NO₂, ammonia, and CO [12,13]. Decorating graphene with

metal nanoparticles (NP) like Au, Pt, Pd, or Ag has been found to enhance the sensitivity to gas molecules due to the catalytic effect of the nanoparticles [14,15].

On the other hand, transition metal dichalcogenides (TMDs) have emerged as an exciting class of 2D materials for gas sensing applications [16–19]. Among the TMDs, molybdenum disulfide (MoS_2) has garnered significant interest and attention due to its exceptional sensing, electronic, optical, and catalytic properties [3,20,21]. MoS_2 is a layered structure, with each layer consisting of covalently bonded Mo-S atoms, and neighboring layers are stacked to each other via van der Waals forces [22]. Bulk MoS_2 has an indirect band gap of 1.2 eV, while, as for the atomically thin MoS_2 sheets, there is a transition to a direct bandgap of 1.8 eV, leading to enhanced charge transport, high specific surface areas due to their sheet-like structures with large basal planes and highly reactive edges, and increased electron concentration at the surface [23]. These properties of MoS_2 make it highly desirable for the development of next-generation memory devices [24], photodetectors [25], solar cells [26], and gas sensors [3,11,27].

Several research works have demonstrated the potential of MoS_2 -based gas sensors for detecting gases like nitrogen dioxide (NO_2) [28], ammonia (NH_3) [29], nitric oxide (NO) [30], and hydrogen [11,18,27]. Duesberg et al. demonstrated the synthesis of MoS_2 patterns and recorded high-sensitivity detection of ammonia with a limit of detection at the ppm level [31]. Zhou et al. reported Schottky-contact MoS_2 -based sensors which are sensitive to 20 ppb and 1 ppm of NO_2 and NH_3 , respectively [32]. Zhang and co-workers presented the influence of the thickness on the performance of MoS_2 gas sensors to NO [33]. Zhou et al. demonstrated a MoS_2 -based sensor with a 92.6% response to 500 ppm of CO at 230 °C [34]. Moreover, Agarwal et al. presented a highly sensitive and fast hydrogen sensor based on monolayer MoS_2 pyramid structures with a 69.1% response to 1% of hydrogen [3].

However, sensors based on bare MoS_2 suffer from sluggish response–recovery speeds and low sensitivity, especially when it comes to the detection of hydrogen gas [3,35]. We have seen that functionalizing the host matrix with a determined noble metal enhances the sensitivity and the selectivity of the sensor to a specific gas. Based on our previous works, we found that CuO nanoparticles are very suitable for the detection of H_2S [36]. Additionally, we showed that Pd/PdO nanoparticles have highly enhanced the sensitivity and selectivity of WO_3 to H_2 [37]. Additionally, it was reported that the incorporation of noble metal nanoparticles onto MoS_2 has shown promise in detecting hydrogen with low power consumption and high sensitivity [9,27,35,38–40]. The improved sensing response attributed to the incorporation of noble metals is a result of electronic sensitization (ES) and chemical sensitization (CS) [41,42]. Electronic sensitization involves the oxidized form of the noble metal creating electron-depletion layers (EDLs) at the interface between the noble metal and the sensing layer [41,43], while chemical sensitization arises from a catalytic surface reaction in which noble metals offer low energy sites for the gas adsorption, leading to enhanced sensor sensitivity via a spillover process [41,44]. Noble metal decoration not only enhances sensitivity and helps in decreasing the optimal sensing temperature but helps in enhancing the long-term stability of the sensors as well [41]. Irrespective of the functionalization process employed, two crucial factors governing noble metal decoration are the amount and the size of the nanoparticles. The optimization of nanoparticle decoration amounts on the sensing layer is important as it directly influences the dissociation of gas molecules. If the decoration is insufficient, the sensitization effect will be diminished. Conversely, excessive decoration would lead to the formation of a continuous film, leading to reduced sensitivity [45].

MoS_2 offers functional groups on both the basal plane and edge sites, which allows for easy incorporation of adatoms on the surface [33,46,47]. The most common method to deposit nanosized metal nanoparticles on MoS_2 using a vacuum is with an e-beam evaporator, as explored by Park et al. to decorate MoS_2 with Pt nanoparticles for NH_3 and H_2S detection [48]. Suh et al. also utilized an e-beam evaporator to decorate Pd and Au on MoS_2 to demonstrate the selectivity of the composite to $\text{C}_2\text{H}_5\text{OH}$, H_2 , NH_3 , and NO_2 [49]. Nonetheless, vacuum-based processes pose drawbacks such as high costs and

power consumption, limiting gas sensor development. Burman et al. employed a solution process using glucose as a reducing agent for Au doping on MoS₂ for detecting ammonia with high sensitivity [50]. Huang et al. took advantage of various capping and reducing agents for the epitaxial growth of Pd, Pt, and Ag metal nanostructures on MoS₂ [51]. The use of reducing agents for nanostructure decorations indeed facilitates the reduction of metal precursors into controllable shapes of metal nanoparticles but may act as a barrier for gas sensing [52]. Kim et al. addressed this issue by using a solution process reaction without reducing agents to decorate 2D MoS₂ nanoflakes with Au, Pt, and Pd for selective ammonia, hydrogen, and ethanol sensing [52]. Lee and co-workers deposited Pt using atomic layer deposition (ALD) on MoS₂ for H₂ sensing [53].

Herein, we report the development of bare and Pd-NP-decorated multilayer MoS₂ for hydrogen sensing. Our method is a simple two-step procedure: (i) airbrushing MoS₂ onto alumina substrates, followed by (ii) low-temperature AACVD decoration of Pd nanoparticles onto MoS₂ sensing layers. To the best of our knowledge, none of the reported works have combined airbrushing and low-temperature AACVD methods to functionalize TMD materials. The sensing materials were characterized with FESEM, HRTEM, XRD, and Raman spectroscopy to study the morphology, crystal structure, and decoration characteristics. We investigated the chemiresistive sensing mechanism of bare and Pd-decorated MoS₂ and studied the impact of Pd decoration on the sensing properties of MoS₂ to hydrogen gas. The sensors display a response of 55% to 100 ppm of hydrogen gas at 150 °C and show a clear impact of Pd decoration on hydrogen sensitivity.

2. Experimental Section

2.1. Materials, Chemicals, and Sensor Fabrication

2.1.1. Materials and Sensor Fabrication

MoS₂ powder (CAS:1317-33-5) was purchased from Sigma-Aldrich, Madrid, Spain and used without further modifications. A total of 20 mg of MoS₂ powders was sonicated in 10 mL of ethanol (Scharlab, Barcelona, Spain CAS: 64-17-5) for 45 min to obtain a homogenous suspension. The suspension was immediately airbrushed onto alumina transducers (Ceram Tech GmbH, Plochingen, Germany) to achieve MoS₂ thin films coating the interdigitated electrode area. Nitrogen was used as a carrier gas during the airbrushing. In order to achieve thin films of reproducible thickness, the resistance of the films was monitored during deposition by connecting the alumina transducer to a multimeter. As soon as the desired resistance of the material was reached, the deposition process was stopped. Samples were fabricated in four sets for each type of material. The average resistance of a pristine set of sensors was 400 MΩ ± 12 MΩ, while, as for sensors with 1 mg of Pd precursor (MoS₂-Pd_1), the average resistance was 72 MΩ ± 4 MΩ. Also, for the sample with 2 mg of Pd precursor (MoS₂-Pd_2), the average resistance was 55 MΩ ± 6 MΩ. All these resistance values were calculated at room temperature. Moreover, the average thickness of the deposited layers was calculated to be around 582 nm using focus ion beam (FIB). The FESEM images of the thickness analysis of the sensing layer are presented in Figure S1.

2.1.2. Pd-Nanoparticle-Decorated MoS₂ Nanosheets Using AACVD Method

Palladium nanoparticles were incorporated onto the fabricated MoS₂ sensors using aerosol-assisted chemical vapor deposition (AACVD). The reaction was performed at comparatively low temperature of 250 °C. To study the effect of Pd concentration on the sensor responses, two amounts of the palladium precursor were used to decorate MoS₂ sensors. In a typical synthesis procedure, 1 mg and 2 mg of Palladium (II) acetylacetonate (Sigma-Aldrich, Madrid, Spain CAS: 14024-61-4) were dissolved in 5 mL methanol (CAS: 67-56-1). The solution was ultrasonicated to ensure full solubilization. The solution was placed in an ultrasonic humidifier to generate aerosol. N₂ gas with a flow of 0.5 L/min was used as a carrier gas to transport the aerosol to the MoS₂ sensors preheated at 250 °C in a hot wall reactor. The AACVD method is similar to our previous reported works [54,55]. The

deposition time was about 5 min; after that, the chamber was left to cool down naturally. The sensors were named according to the Pd decoration concentration, viz., MoS₂-Pd₁ and MoS₂-Pd₂ for 1 mg and 2 mg precursor amounts, respectively.

2.2. Material Characterization Techniques

The morphology of the prepared samples was analyzed using a field emission scanning electron microscope (FESEM-Thermo Scientific Scios 2, Waltham, MA, USA). The FESEM microscope used in this study is equipped with EDX as well to calculate the wt. % of palladium nanoparticles. Moreover, the FESEM equipment is also equipped with the focus ion beam (FIB) tool used here to calculate the thickness of the sensing layer. The crystal structure was analyzed via X-ray diffraction using a Bruker AXS D8 diffractometer equipped with parallel incident beam (Gobel mirror) vertical θ - θ goniometer, XYZ motorized stage, and with a GADDS (General Area Diffraction System). A JEOL F200 TEM ColdFEG (JEOL, Tokyo, Japan) operated at 200 kV was used for the high-resolution transmission electron microscopy (HRTEM) characterization. EDX spectra and elemental analysis was performed using the same HRTEM equipment. The Raman spectra were recorded using a Renishaw in Via, laser 514 nm, ion argon-Novatech, 25 mW.

2.3. Gas Sensing Measurements

The gas sensing measurements were conducted using a homemade detection system in a Teflon[®] chamber with a volume of 35 mL. The chamber is designed to accommodate four sensors simultaneously. The chamber consists of an inlet connected to the gas delivery system and an outlet which is connected to the exhaust. Commercial alumina substrates with interdigitated platinum electrodes (300 μ m electrode gap) on the front side and a platinum resistive meander on the back side were used to deposit the sensing material. The sensor responses were recorded by monitoring the sensing material resistance using an Agilent-34972A data acquisition system. Calibrated cylinders of NO₂ (total concentration, 1 ppm), H₂ (total concentration, 1000 ppm), NH₃ (total concentration, 100 ppm), CO (total concentration, 100 ppm), and benzene (total concentration, 10 ppm) were mixed with pure synthetic air using Bronkhorst mass-flow controllers. A constant flow rate of 100 mL min⁻¹ was maintained during all the experiments. The sensors were exposed to the analyte gas for 10 min and subsequently cleaned in dry air for 60 min. The cleaning time to recover the baseline was adapted according to the sensor operating temperature; 60 min for 50 °C, 100 °C, and 150 °C and 120 min for room temperature operation. Prior to gas sensing measurements, sensors were kept under a constant flow of dry air for a minimum of 5 h to completely stabilize their initial baseline resistance. The sensor responses were calculated using Equation (1) for reducing gas species and Equation (2) for oxidizing gas species.

$$\left(\frac{R_{gas} - R_{air}}{R_{air}} \times 100\right) \% \quad (1)$$

$$\left(\frac{R_{air} - R_{gas}}{R_{air}} \times 100\right) \% \quad (2)$$

where R_{air} and R_{gas} are the real-time resistances of the sensor exposed to air and to analyte, respectively.

3. Results and Discussions

3.1. Material Characterization

3.1.1. FESEM Analysis

Figure 1 depicts the FESEM images of the sensing materials. Upon analysis, it is evident that the deposited MoS₂ exhibits a multilayered structure, as shown in Figure 1a. The size of the MoS₂ structures varies from 200 nm to 1.5 μ m (edge to edge), displaying clear and distinct ridges. In the case of MoS₂-Pd₁, most of the decorated Pd nanoparticles are spherical with an average size of 15 nm, as shown in Figure 1b. In the case of MoS₂-Pd₂,

the decorated nanoparticles are a mix of spherical and rice-grain shaped with an average size slightly larger (23 nm) than that observed in MoS₂-Pd₁, as illustrated in Figure 1c. Decorating with a higher concentration of palladium leads to higher coverage, which can be seen in the FESEM images. Different Pd decoration amounts were used to check the impact of the decoration amount on the gas sensing properties of the material. The decoration of the sensors was kept at low concentrations to avoid hindering the transport of dissociated hydrogen atoms to the MoS₂ channel. This could be owed to the hampering of the catalytic effect due to the increased concentration of Pd [53]. Moreover, it is clear that the deposition of metal nanoparticles has no visible influence on the morphology of the MoS₂. Also, an Energy Dispersive X-ray Analysis (EDX) of the samples was conducted to determine the average weight percentage (wt. %) of Palladium (Pd) in the respective samples. The EDX analysis was carried out at various spots on the samples; the resulting data were analyzed to calculate the average wt. % of palladium. Based on the calculations, the average wt. % of Pd in the MoS₂-Pd₁ sample was 7.27 wt. %, while, as in the MoS₂-Pd₂ sample, the wt. % of palladium was 11.69 wt. %.

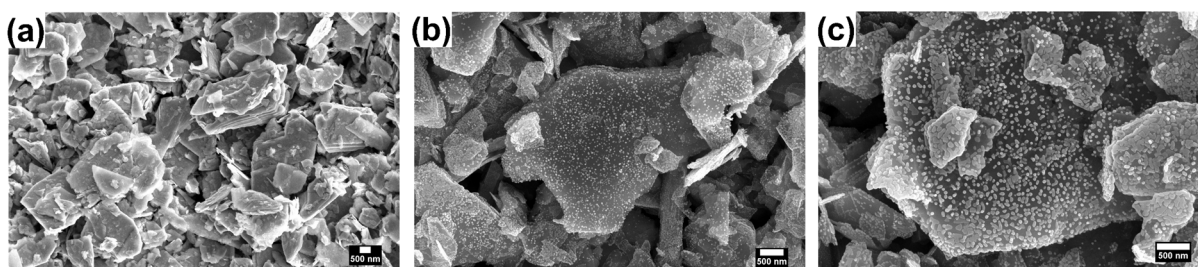


Figure 1. FESEM images of (a) MoS₂, (b) MoS₂-Pd₁, and (c) MoS₂-Pd₂.

3.1.2. HRTEM Analysis

Supplementing the FESEM morphological data, an HRTEM analysis of one of the sensing materials, MoS₂-Pd₂, was performed combined with EDX spectroscopy. Pd-decorated MoS₂ films were scraped off the alumina substrate and drop-casted over carbon-coated copper grids. Analysis of the HRTEM results reveals the crystalline layered structure of the MoS₂ with successful Pd decoration, as shown in Figure 2a,b. At some places, the layers are randomly oriented, while at other places the layers are stacked one on other. EDX spectra and HRTEM images of the sensing material are presented in Figure 2c–e, respectively. EDX analysis revealed the presence of Pd nanoparticles on MoS₂ sheets. Upon further analysis, we verified the interlayer distance, with d equal to 0.215 nm corresponding to the (103) plane of MoS₂ (ICDD card number: 65-1951) as shown in Figure 2d. The d -spacing calculated for Pd nanoparticles is 0.232 nm, which corresponds to the (111) plane of Pd (ICDD card number 88-2335). The interlayer distance results of both MoS₂ and palladium were confirmed with XRD analysis.

3.1.3. XRD

The crystal structure of the sensing films was analyzed using an X-ray diffraction (XRD) method. Figure 3 shows the XRD diffractogram recorded from pristine MoS₂ and Pd-decorated MoS₂ in the range of $2\theta = 5^\circ$ to 80° . The observed diffraction peaks match with the hexagonal phase of MoS₂ (ICDD card number: 65-1951) with lattice constants $a = 0.316$ nm and $c = 1.2294$ nm belonging to the P63/mmc space group. The major diffraction peaks can be indexed to the (002) at 14.42° , (102) at 35.88° , (103) at 39.56° , and (105) at 49.81° lattice planes. Some additional peaks are observed in Figure 3b,c. These peaks can be indexed to palladium (ICDD card number: 88-2335). The diffraction peaks of palladium match the cubic phase with lattice constant $a = 0.39$ nm (Fm-3m space group). At $2\theta = 40.01$, 46.53 , and 67.92 , the peaks of MoS₂ and Al₂O₃ almost coincide with the peaks of Pd. Hence, in Figure 3b,c, the peaks are more intense than those in Figure 3a, which corresponds to pristine MoS₂. This confirms the presence of Pd decorating the surface of MoS₂.

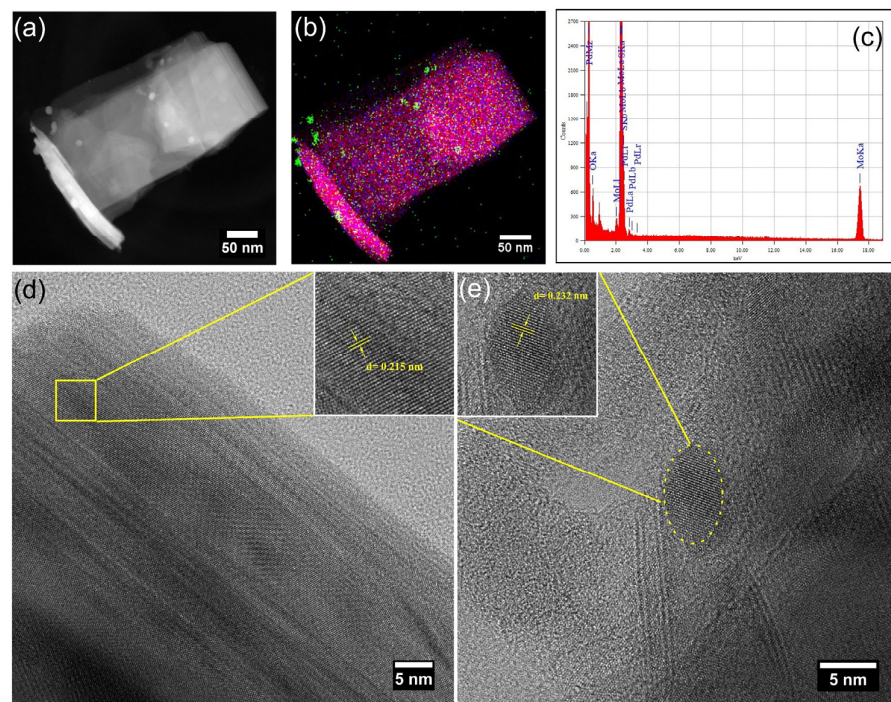


Figure 2. (a) TEM image of multilayer MoS₂-Pd, (b) color mapping of MoS₂-Pd, (c) EDX pattern of MoS₂-Pd, (d) HRTEM image of multilayer pristine MoS₂ with d-spacing of 0.215 nm, (e) close-up of Pd nanoparticle with d-spacing 0.232 nm.

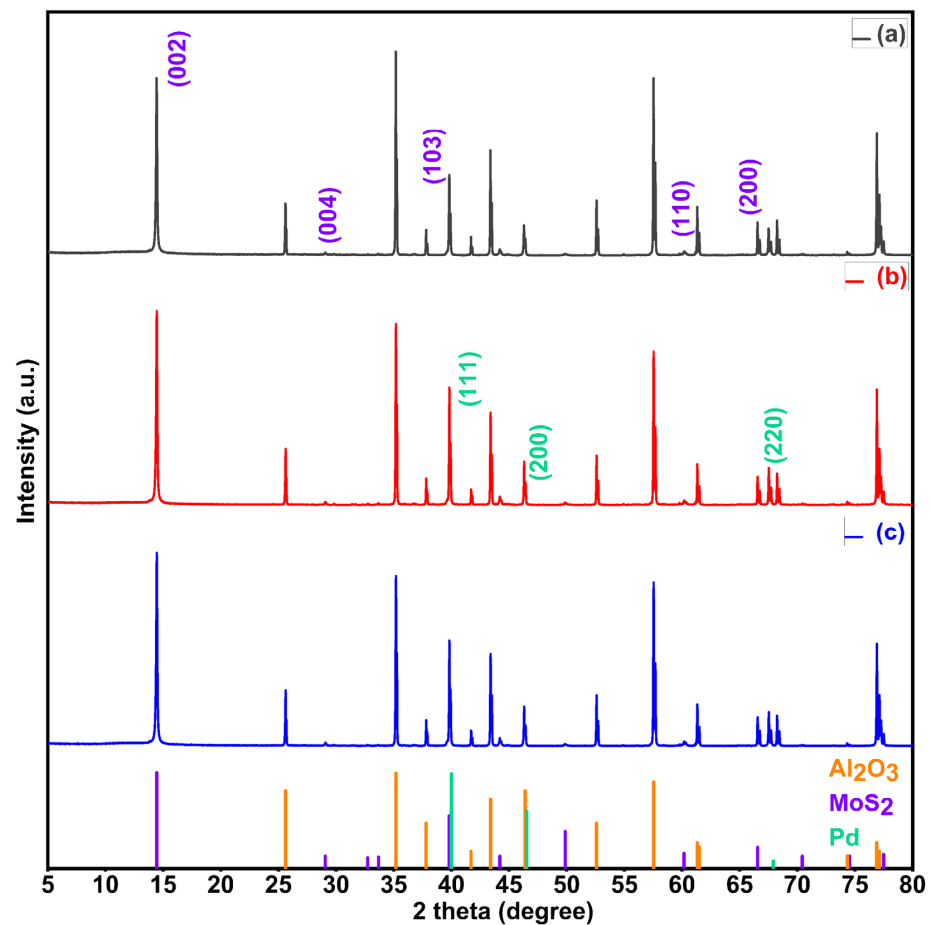


Figure 3. XRD diffractogram of (a) MoS₂, (b) MoS₂-Pd₁, and (c) MoS₂-Pd₂.

3.1.4. Raman Spectroscopy

Figure 4 shows the typical Raman spectra of pristine and Pd-decorated MoS₂. The Raman spectra of all the samples show peaks near 400 cm⁻¹, which confirms the 2H phase of MoS₂. The two characteristic peaks signify the vibration modes for MoS₂: E_{2g}¹, which corresponds to in-plane vibration of the molybdenum atom and is opposite to two sulfur atoms, and A_{1g}, mode which corresponds to the out-of-plane vibration of sulfur atoms (Mo atom being immobile) [56]. In addition to the main characteristic peaks, the small peak at ~283 cm⁻¹ can be assigned to the MoO₂ phase [57,58]. Table 1 summarizes the Raman peak positions of all the samples. The values of Δ provide the information about the number of layers in the MoS₂. As can be seen from the table, Δ ≥ 25, indicating the multilayered structure of MoS₂ [59,60]. This is in agreement with the FESEM and HRTEM results.

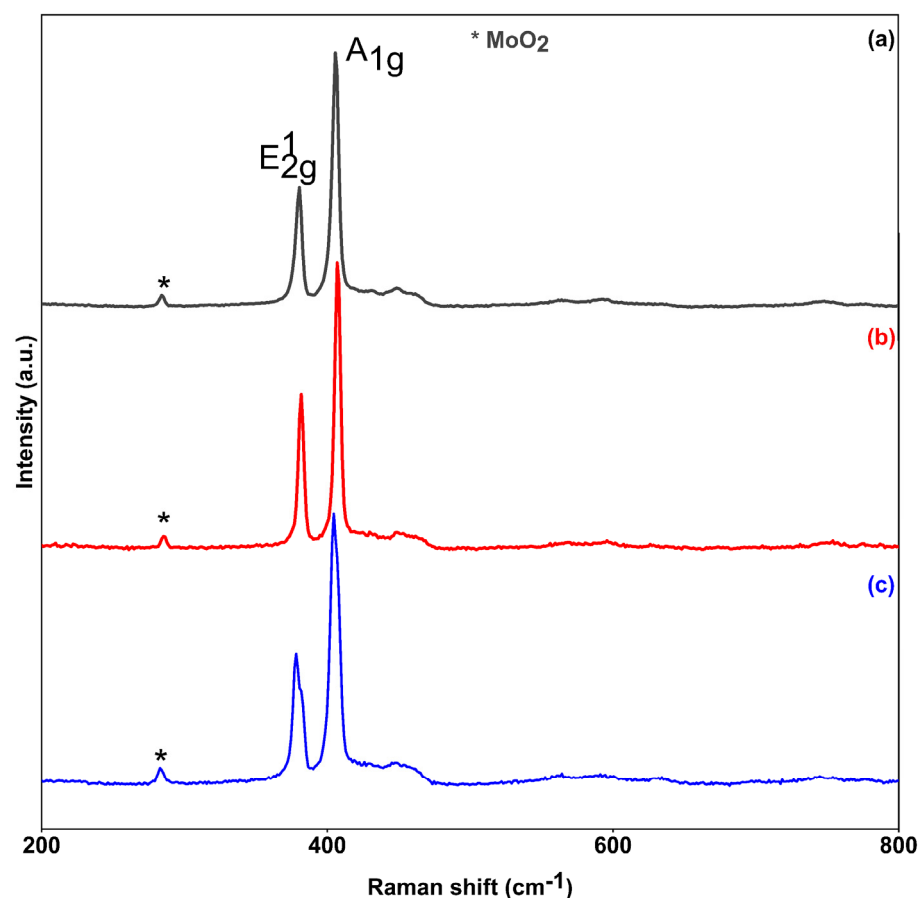


Figure 4. Raman spectra of (a) MoS₂, (b) MoS₂-Pd₁, and (c) MoS₂-Pd₂.

Table 1. Summary of Raman data.

Sample	E _{2g} ¹	A _{1g}	Δ = (A _{1g} - E _{2g} ¹)
MoS ₂	381	406	25
MoS ₂ -Pd ₁	381	407	26
MoS ₂ -Pd ₂	378	405	27

3.2. Gas Sensing Results

3.2.1. Hydrogen Gas Sensing

The gas sensing characteristics of pristine and Pd-decorated MoS₂ thin films were analyzed to hydrogen gas. The sensor responses were checked at different operating temperatures (room temperature, 50 °C, 100 °C, and 150 °C) to study the optimal working temperature. Optimal temperature is an important parameter to define thermally active

interactions between the target gas molecules and the adsorbed oxygen ionic species. Operating temperature plays an important role in determining the gas sensing performance of the sensors as it directly affects the selectivity, sensitivity, and response/recovery time. The desorption rate of the reacted by-products surpasses the adsorption rate of the target gas as temperature increases, reaching the peak efficiency at the optimal working temperature [61]. Figure 5 shows the sensor responses to 100 ppm H₂ with respect to increases in temperature. The sensor responses increase with increases in the temperature, showing maximum response at 150 °C. Thus, the optimal working temperature of the sensors is 150 °C. The sensors were not operated beyond 150 °C to avoid the risk of oxidizing MoS₂ to MoO_x [62]. Indeed, based on our previous studies regarding the long-term stability of TMD-based gas sensors operated at temperatures equal to or below 150 °C, there were no remarkable changes in the material characteristics or the gas sensing performances. It is clear from the figure that there is a significant increase in the sensor response from pristine MoS₂ to Pd-decorated MoS₂, specifically in the case of MoS₂-Pd₁. All three sensors showed reproducible responses. The sensor responses were calculated to be 55% at 150 °C to 100 ppm of H₂ for MoS₂-Pd₁, which is 1471% higher than the responses recorded in the case of pristine MoS₂. Also, in the case of MoS₂-Pd₂, the response is 300% higher than that for the pristine MoS₂ sensor. As is evident from Figure 5, the minimum response recorded in the case of MoS₂-Pd₁ is 14.3% at room temperature, which is 2760% higher than that of the pristine MoS₂ under the same conditions. We can clearly observe the impact of Pd decoration on the sensitivity of the sensors to H₂ gas. The main reason behind this increase in the sensitivity is the reaction between Pd and H₂ atoms generating palladium hydride (PdH_x) at room temperature [63,64] and also the affinity of MoS₂ for H atoms [65]. Moreover, Pd nanoparticles have one of the highest sticking and diffusion coefficients [66]. Therefore, the results confirm the synergistic contribution of Pd and MoS₂ for H₂ sensing. The dynamics of resistance change and baseline recovery for all the sensors in a hydrogen environment as well as in synthetic air are shown in Figure 6. The amount of Pd decoration has a clear impact on the response of the sensors to hydrogen. Higher Pd coverage leads to the formation of more Schottky barriers, which, in turn, increases the resistance. In our case, we found the baseline resistance of the sensors with higher Pd decoration approximately 1 MΩ higher than the sensors with low Pd decoration (Figure 6b,c). When exposed to air, Pd tends to oxidize and form PdO nanoparticles, a p-type semiconductor. The decrease in the baseline resistance indicates that PdO nanoparticles inject holes in the MoS₂ films. Moreover, excessive decoration of Pd on MoS₂ impedes the transport efficiency of dissociated hydrogen atoms to the MoS₂ channel, consequently hindering the catalytic effect. Furthermore, abundant Pd decoration leads to a reduction in the available surface area of MoS₂ for interactions with hydrogen gas species owing to increased coverage by Pd nanoparticles. This results in lower sensing characteristics of the MoS₂, suggesting lower Pd decoration amounts [41]. We compared our sensor responses with the highest-performing sensors in the literature based on noble metals and MoS₂. Our sensors outperform the sensors in every aspect. Table 2 shows the comparison of our sensors with some highly responsive MoS₂-based sensors for hydrogen sensing.

Table 2. Hydrogen gas sensing comparison of various noble metal-doped/decorated MoS₂ sensors.

Gas Sensing Material	Concentration	Response Calculation Formula	Response %	Operating Temperature	Reference
ALD Pt-decorated MoS ₂ nanosheets	1000 ppm	$\frac{R_{air}}{R_{H_2}}$	440	250 °C	[53]
Pd nanoclusters–MoS ₂ heterostructure	140 ppm	$\frac{R_{H_2} - R_{air}}{R_{air}} \times 100$	17	RT (with light activation)	[9]
Pd-functionalized MoS ₂ nanosheet	10,000 ppm	$\frac{R_{H_2} - R_{air}}{R_{air}} \times 100$	35.3	RT	[38]

Table 2. Cont.

Gas Sensing Material	Concentration	Response Calculation Formula	Response %	Operating Temperature	Reference
Pt-decorated MoS ₂ hollow structures	40,000 ppm	$\frac{R_{H_2} - R_{air}}{R_{air}} \times 100$	11.2	RT	[63]
Pd-functionalized edge-enriched MoS ₂	500 ppm	$\frac{R_{H_2} - R_{air}}{R_{air}} \times 100$	33.7	RT	[67]
Pd-decorated MoS ₂	100 ppm	$\frac{R_{H_2} - R_{air}}{R_{air}} \times 100$	55	150 °C	This work
			14.9	RT	

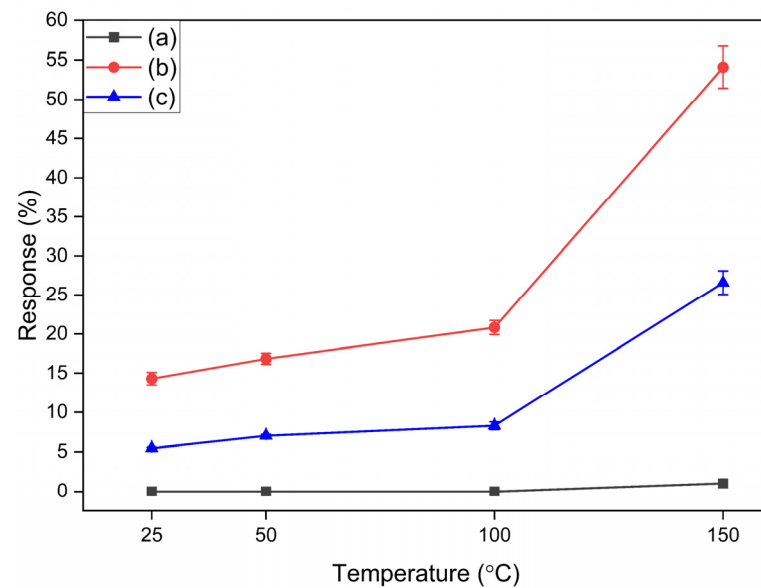


Figure 5. Sensor responses as a function of temperature to 100 ppm H₂, (a) MoS₂, (b) MoS₂-Pd₁, and (c) MoS₂-Pd₂.

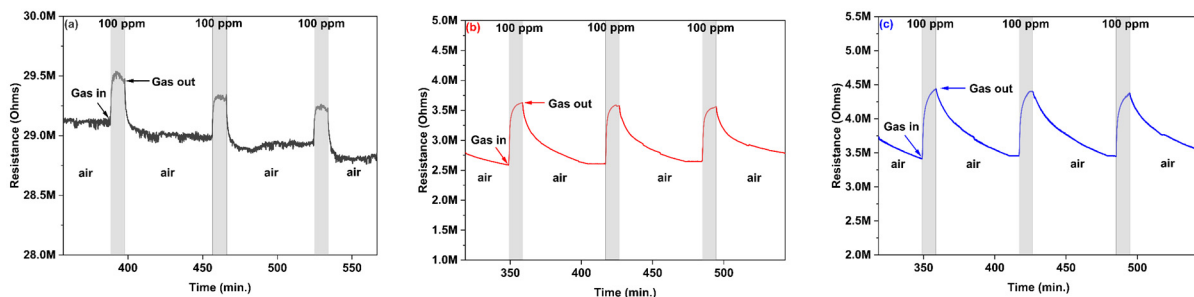


Figure 6. Sensor resistance dynamics (a) MoS₂, (b) MoS₂-Pd₁, and (c) MoS₂-Pd₂ to 100 ppm H₂ at 150 °C.

The increase in the electrical resistance values of the sensors upon exposure to hydrogen molecules (reducing gas) indicates the p-type nature of both the pristine and Pd-decorated sensors. Also, the sensors were exposed to increasing concentrations of H₂ ranging from 50 ppm to 500 ppm in a background of dry air. Figure 7 show the resistance change dynamics of the sensors to increasing H₂ pulses while being operated at 150 °C. As can be seen in the figure, the sensors responded well to the respective hydrogen concentrations with almost complete baseline recovery except in the case of pristine MoS₂, which shows a slight drift. The sensors were able to detect a very low concentration of 50 ppm of H₂ with excellent sensitivity. Rapid changes in the sensing signals exceeding final steady-state values can be seen in Figure 7b,c. This can be owed to the competition

between reaction speed and gas diffusion [68–70]. The phenomenon is prominent when H_2 concentration is high or Pd decoration is in excess. That is why this is much more prominent in the sensor with higher Pd content, as depicted in Figure 7c. To suppress this issue, when sensing higher concentrations of H_2 , thinner materials with high porosity can be helpful [63]. Figure 8 shows the sensor response as a function of the hydrogen concentration. The Pd-decorated sensor response values saturate above 100 ppm, and up to 100 ppm, the relationship between the sensor responses and the H_2 concentration is quite linear. Also, the sensor responses with respect to H_2 concentration in the case of pristine MoS_2 are linear. It is worth mentioning that 100 ppm is much below the permissible limit for H_2 gas for safety purposes. Palladium facilitates the dissociation of hydrogen molecules into chemisorbed hydrogen atoms (H) on its surface under ambient conditions without encountering any significant barriers. After their formation, these atoms quickly saturate the surface and migrate into interstitial lattice sites in the subsurface region before finally diffusing into the bulk. The diffusion of H atoms is impeded by an energy landscape characterized by subsurface sites that are energetically more favorable compared with bulk interstitials. Therefore, it is safe to assume that subsurface sites are occupied irrespective of the hydrogen concentration in the bulk. Additionally, it has been demonstrated that the presence of hydrogen in the subsurface layer can lead to the generation of lattice strain, which can impact the thermodynamics of the sorption process in nanoscale systems like nanoparticles [71].

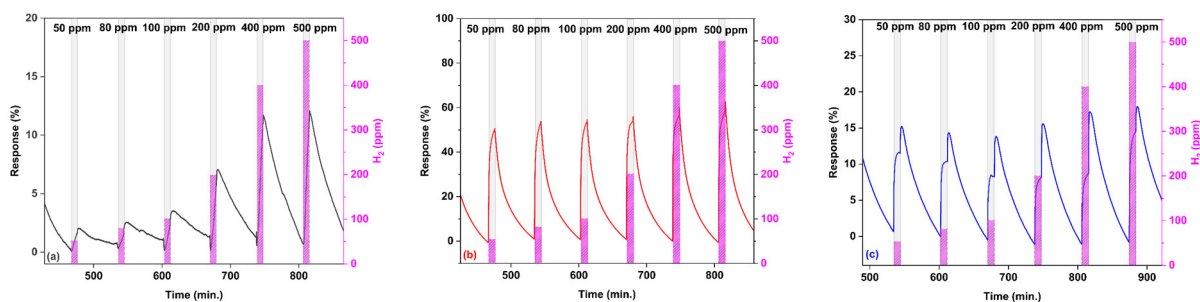


Figure 7. Sensor responses to increasing concentration of H_2 at 150 °C (a) MoS_2 , (b) MoS_2 -Pd₁, and (c) MoS_2 -Pd₂.

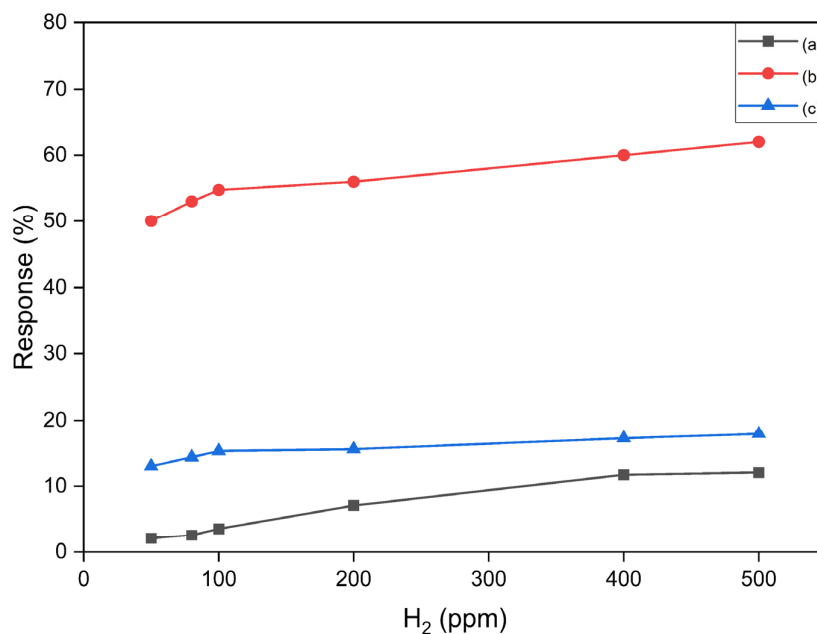


Figure 8. Calibration curves to H_2 for the different types of sensors tested. Sensors operated at 150 °C, (a) MoS_2 , (b) MoS_2 -Pd₁, and (c) MoS_2 -Pd₂.

3.2.2. Selectivity Test

In addition to H₂ gas, the gas sensing performance of MoS₂ and Pd-decorated MoS₂ was investigated to reducing gases such as CO, NH₃, ethanol, and benzene. Also, the sensor responses were investigated against an oxidizing gas: NO₂. The typical resistance response dynamics for 5 ppm benzene, 80 ppm CO, 10 ppm ethanol, and 5 ppm NH₃ are shown in Figures S2, S3, S4, and S5, respectively (supporting information). The histogram in Figure 9 summarizes the sensing results analyzed for each gas. Decorating MoS₂ with Pd clearly enhances the response to H₂ and diminishes cross-sensitivity to carbon monoxide, ammonia, benzene, and ethanol. However, all the sensors respond to NO₂ with a significant response. It is worth mentioning and stressing that 800 ppb of NO₂ is a very high concentration. The United States Environmental Protection Agency (U.S. EPA) has regulated the limit of exposure of NO₂ at less than 100 ppb, keeping in view its negative effects both on the environment and human life [72]. For NO₂ concentrations of 100 ppb, the sensor response is 18%. The pristine MoS₂ demonstrates a robust response to NO₂, while it lacks sensitivity to H₂. By combining these two distinct sensors, we anticipate that the composite system can effectively mitigate the issue of cross-sensitivity displayed by Pd-decorated MoS₂ to NO₂. The complementary nature of the individual sensors, with pristine MoS₂ being selective to NO₂ and Pd-decorated MoS₂ being responsive to H₂, allows for a synergistic response that can enhance the discrimination capabilities of the composite sensor. This combination holds promise in suppressing the undesired cross-sensitivity exhibited by the Pd-decorated MoS₂ sensor to NO₂, enabling more accurate and reliable gas sensing applications. All the interfering species were tested at significantly higher concentrations; hence, it can be derived that Pd decoration improved selectivity to H₂.

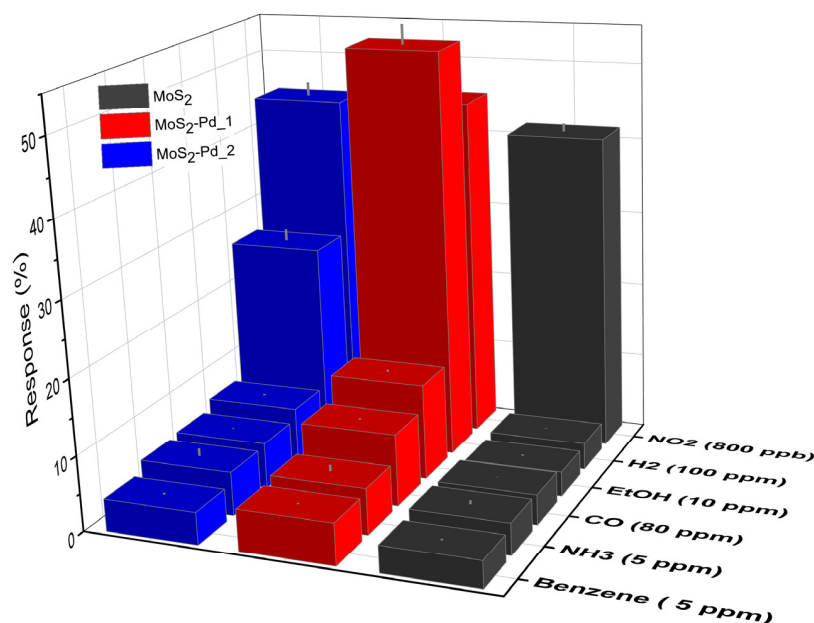


Figure 9. Response histogram of MoS₂, MoS₂-Pd₁, and MoS₂-Pd₂ to NO₂ (800 ppb), H₂ (100 ppm), ethanol (10 ppm), carbon monoxide (80 ppm), ammonia (5 ppm), and benzene (5 ppm) at 150 °C.

Ambient moisture affects the electrical properties of gas sensors dramatically and ultimately impacts the sensitivity heavily. This makes it mandatory to evaluate the behavior of the gas sensors in humid environments. Figure 10 depicts the sensor responses to 5 ppm of benzene (a reducing gas) under dry air and at 50% relative humidity (at 25 °C). Also, Figure S6 illustrates the normalized sensor resistance changes as a function of time. Analysis of the results reveals an overall decrease in the baseline resistance of the sensing layer when exposed to a humid environment. This has been reported in metal oxide semi-conducting materials as well [73]. We noticed a slight increase in the sensor responses, except in the MoS₂-Pd₂ sensor. Generally, in humid environments, the water vapors (hydroxyl group)

and the target gas molecules enter a competition at the active sites. The impact of the humidity is much more prominent when the relative surface distribution of the hydroxyl groups is much higher than the oxygen species [60]. The obtained results indicate that the sensors exhibit strong resilience to high levels of moisture.

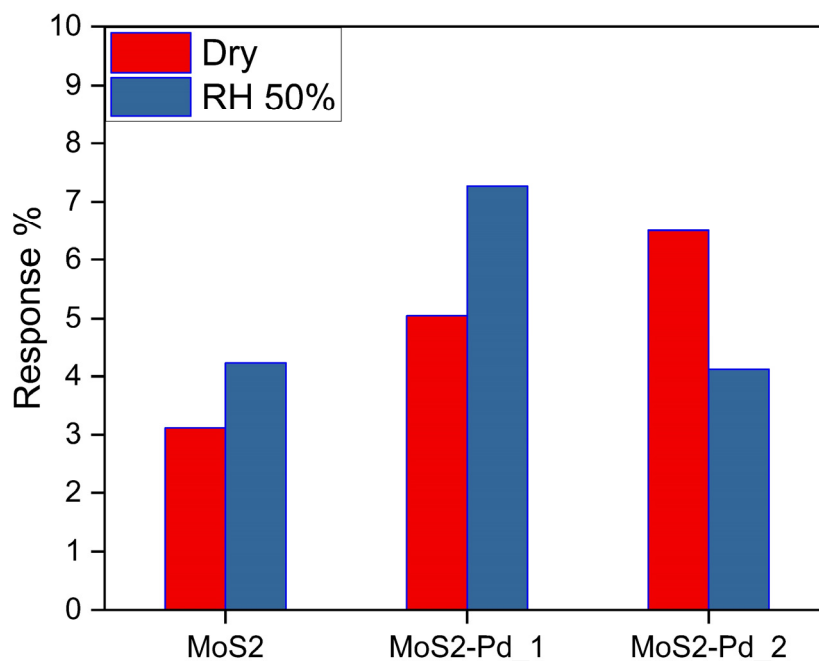
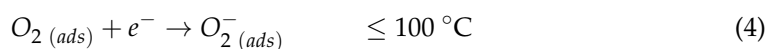


Figure 10. Sensor responses to 5 ppm benzene at 150 °C.

3.2.3. Hydrogen Gas Sensing Mechanism

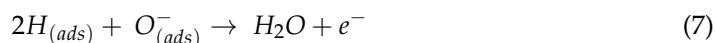
The sensing mechanism of chemoresistive gas sensors is based on electrical resistance modulation, which can be attributed to the interactions occurring on the sensor substrate because of the chemical reactions between the sensor surface and target gas [74]. When a sensor surface interacts with hydrogen, a reducing gas, it donates electrons upon adsorption. Depending on the type of the material (n-type or p-type), the transferred electrons lead to an increase or decrease in the electrical resistance of the material [39,40,75,76]. In this work, the resistance of MoS₂ increased upon exposure to H₂, indicating the p-type behavior of the material.

When the sensors are exposed to air, the oxygen molecules dissociate on the MoS₂ surface, resulting in the formation of adsorbed oxygen species like (O₂⁻ and O⁻) at elevated temperatures [39], as is shown in Equations (3) and (4).



Pd nanoparticle addition promotes the gas sensing ability of MoS₂ by acting as an electronic sensitizer while sensing H₂. Pd enhances the sensor responses by increasing the rate of chemical processes. One of the main roles of the Pd is to make catalytic oxidation easy on the MoS₂ active layer [39]. When the sensors are exposed to hydrogen, the Pd nanoparticles provide adsorption sites for hydrogen molecules, as seen in Equation (5). Pd decoration enables barrierless dissociation of hydrogen molecules (H₂) into chemisorbed hydrogen atoms (H) on its surface. The dissociation of the adsorbed hydrogen molecules takes place to form hydrogen atoms (Equation (6)). This process is known as the spillover effect of Pd catalysts with respect to H₂ sensing [63]. For Pd particles larger than 5 to 10 nm (as in our case), the diffusion lengths for H atoms to reach the core are shorter [77]. The hydrogen atoms react with the O⁻ oxygen species (Equation (7)), facilitating the electrons to

the sensor. These electrons combine with holes and reduce the charge carrier concentration, eventually leading to the increase in the sensor resistance. This increase is proportional to the concentration of hydrogen gas. These reactions are facilitated by the presence of Pd nanoparticles in the matrix owing to their strong affinity for the mitigation of chemisorbed gaseous species.



4. Conclusions

In this paper, layered MoS₂ was successfully deposited onto alumina substrates. AACVD at 250 °C was employed for the Pd decoration of MoS₂. The sensing material was well characterized using FESEM, XRD, HRTEM, and Raman spectroscopy. Multilayered crystalline MoS₂ sheets were observed with homogenous Pd nanoparticle decoration. The size of the Pd nanoparticles was between 15 nm and 23 nm. The gas sensing results of bare and Pd-decorated MoS₂ to H₂ were analyzed. The Pd-nanoparticle-decorated MoS₂ sensing layer acts as an active hydrogen-sensing layer with a maximum response of 55% at 150 °C to 100 ppm of H₂. The sensors show high resilience to humidity, as the sensor responses increase slightly when exposed to 50% relative humidity. The effect of Pd decoration is evident with the sensitivity of the sensors depending on the amount of Pd decoration. A combined bare and Pd-decorated MoS₂ sensor system holds promise for achieving a highly sensitive and selective H₂ detection.

Supplementary Materials: The following supporting information can be downloaded at: <https://www.mdpi.com/article/10.3390/chemosensors11110550/s1>, Figure S1 depicts the thickness of the sensing layer, Figures S2–S5 show resistance dynamics towards interfering gases and Figure S6 shows normalized resistance dynamics in humid environment.

Author Contributions: Conceptualization, S.B.M.; Methodology, S.B.M. and F.E.A.; Validation, E.L.; Formal analysis, S.B.M.; Investigation, S.B.M. and F.E.A.; Writing—original draft, S.B.M.; Writing—review & editing, F.E.A.; Visualization, F.E.A.; Supervision, F.E.A. and E.L.; Funding acquisition, E.L. All authors have read and agreed to the published version of the manuscript.

Funding: This research was funded by Martí-Franquès Research grants Programme (Grant Number: 2019PMF-PIPF-14), Agencia Estatal de Investigación (Grant Number: TED2021-131442B-C31), and AGAUR (Grant Number: 2021 SGR 00147).

Institutional Review Board Statement: Not applicable.

Informed Consent Statement: Not applicable.

Data Availability Statement: Raw data is available from the authors upon request.

Acknowledgments: S.B.M is supported by the Martí-Franquès Research grant Programme, Doctoral grants—2019, (2019PMF-PIPF-14). F.E.A. is a Juan de la Cierva incorporacion Post-Doctoral Fellow. E.L. is supported by the Catalan Institution for Research and Advanced Studies via the 2018 Edition of the ICREA Academia Award. This work is supported by the Agencia Estatal de Investigación (AEI) under grant no. TED2021-131442B-C31 and by AGAUR under grant no. 2021 SGR 00147. The HRTEM was partially funded by the operative program FEDER Catalunya 2014-2020 (IU16-015844).

Conflicts of Interest: The authors declare no conflict of interest.

References

- Jacobson, M.Z.; Colella, W.G.; Golden, D.M. Cleaning the Air and Improving Health with Hydrogen Fuel-Cell Vehicles. *Science* **2005**, *308*, 1901–1905. [[CrossRef](#)] [[PubMed](#)]
- van Renssen, S. The hydrogen solution? *Nat. Clim. Chang.* **2020**, *10*, 799–801. [[CrossRef](#)]

3. Agrawal, A.V.; Kumar, R.; Yang, G.; Bao, J.; Kumar, M.; Kumar, M. Enhanced adsorption sites in monolayer MoS₂ pyramid structures for highly sensitive and fast hydrogen sensor. *Int. J. Hydrog. Energy* **2020**, *45*, 9268–9277. [[CrossRef](#)]
4. Almaev, A.; Nikolaev, V.; Yakovlev, N.; Butenko, P.; Stepanov, S.; Pechnikov, A.; Scheglov, M.; Chernikov, E. Hydrogen sensors based on Pt/ α -Ga₂O₃:Sn/Pt structures. *Sens. Actuators B Chem.* **2022**, *364*. [[CrossRef](#)]
5. Gurlo, A. Nanosensors: Towards morphological control of gas sensing activity. SnO₂, In₂O₃, ZnO and WO₃ case studies. *Nanoscale* **2010**, *3*, 154–165. [[CrossRef](#)] [[PubMed](#)]
6. Liu, X.; Ma, T.; Pinna, N.; Zhang, J. Two-Dimensional Nanostructured Materials for Gas Sensing. *Adv. Funct. Mater.* **2017**, *27*. [[CrossRef](#)]
7. Raza, M.H.; Movlaee, K.; Leonardi, S.G.; Barsan, N.; Neri, G.; Pinna, N. Gas Sensing of NiO-SCCNT Core-Shell Heterostructures: Optimization by Radial Modulation of the Hole-Accumulation Layer. *Adv. Funct. Mater.* **2019**, *30*. [[CrossRef](#)]
8. Zhang, J.; Liu, X.; Neri, G.; Pinna, N. Nanostructured Materials for Room-Temperature Gas Sensors. *Adv. Mater.* **2015**, *28*, 795–831. [[CrossRef](#)]
9. Mai, H.D.; Jeong, S.; Nguyen, T.K.; Youn, J.-S.; Ahn, S.; Park, C.-M.; Jeon, K.-J. Pd Nanocluster/Monolayer MoS₂ Heterojunctions for Light-Induced Room-Temperature Hydrogen Sensing. *ACS Appl. Mater. Interfaces* **2021**, *13*, 14644–14652. [[CrossRef](#)]
10. Matte, H.S.S.R.; Gomathi, A.; Manna, A.K.; Late, D.J.; Datta, R.; Pati, S.K.; Rao, C.N.R. MoS₂ and WS₂ Analogues of Graphene. *Angew. Chem. Int. Ed.* **2010**, *49*, 4059–4062. [[CrossRef](#)]
11. Lee, Y.-H.; Zhang, X.-Q.; Zhang, W.; Chang, M.-T.; Lin, C.-T.; Chang, K.-D.; Yu, Y.-C.; Wang, J.T.-W.; Chang, C.-S.; Li, L.-J.; et al. Synthesis of Large-Area MoS₂ Atomic Layers with Chemical Vapor Deposition. *Adv. Mater.* **2012**, *24*, 2320–2325. [[CrossRef](#)]
12. Li, W.; Geng, X.; Guo, Y.; Rong, J.; Gong, Y.; Wu, L.; Zhang, X.; Li, P.; Xu, J.; Cheng, G.; et al. Reduced Graphene Oxide Electrically Contacted Graphene Sensor for Highly Sensitive Nitric Oxide Detection. *ACS Nano* **2011**, *5*, 6955–6961. [[CrossRef](#)] [[PubMed](#)]
13. Lu, G.; E Ocola, L.; Chen, J. Reduced graphene oxide for room-temperature gas sensors. *Nanotechnology* **2009**, *20*, 445502. [[CrossRef](#)]
14. Gutiérrez, A.; Hsia, B.; Sussman, A.; Mickelson, W.; Zettl, A.; Carraro, C.; Maboudian, R. Graphene decoration with metal nanoparticles: Towards easy integration for sensing applications. *Nanoscale* **2011**, *4*, 438–440. [[CrossRef](#)] [[PubMed](#)]
15. Hashtroudi, H.; Yu, A.; Juodkakis, S.; Shafiei, M. Two-Dimensional Dy₂O₃-Pd-PDA/rGO Heterojunction Nanocomposite: Synergistic Effects of Hybridisation, UV Illumination and Relative Humidity on Hydrogen Gas Sensing. *Chemosensors* **2022**, *10*, 78. [[CrossRef](#)]
16. Geim, A.K.; Novoselov, K.S. The rise of graphene. *Nat. Mater.* **2007**, *6*, 183–191. [[CrossRef](#)]
17. Radisavljevic, B.; Radenovic, A.; Brivio, J.; Giacometti, V.; Kis, A. Single-layer MoS₂ transistors. *Nat. Nanotechnol.* **2011**, *6*, 147–150. [[CrossRef](#)]
18. Sarkar, D.; Xie, X.; Kang, J.; Zhang, H.; Liu, W.; Navarrete, J.; Moskovits, M.; Banerjee, K. Functionalization of Transition Metal Dichalcogenides with Metallic Nanoparticles: Implications for Doping and Gas-Sensing. *Nano Lett.* **2015**, *15*, 2852–2862. [[CrossRef](#)]
19. Xie, X.; Sarkar, D.; Liu, W.; Kang, J.; Marinov, O.; Deen, J.; Banerjee, K.; Engineering, C.; Barbara, S.; States, U. Low-Frequency Noise in Bilayer MoS₂. *ACS Nano* **2014**, *8*, 5633–5640. [[CrossRef](#)]
20. Siao, M.D.; Shen, W.C.; Chen, R.S.; Chang, Z.W.; Shih, M.C.; Chiu, Y.P.; Cheng, C.-M. Two-dimensional electronic transport and surface electron accumulation in MoS₂. *Nat. Commun.* **2018**, *9*, 1–12. [[CrossRef](#)]
21. Mennel, L.; Furchi, M.M.; Wachter, S.; Paur, M.; Polyushkin, D.K.; Mueller, T. Optical imaging of strain in two-dimensional crystals. *Nat. Commun.* **2018**, *9*, 516. [[CrossRef](#)] [[PubMed](#)]
22. Eda, G.; Yamaguchi, H.; Voiry, D.; Fujita, T.; Chen, M.; Chhowalla, M. Photoluminescence from Chemically Exfoliated MoS₂. *Nano Lett.* **2011**, *11*, 5111–5116. [[CrossRef](#)] [[PubMed](#)]
23. Winkler, C.; Harivyasi, S.S.; Zojer, E. Controlling the electronic properties of van der Waals heterostructures by applying electrostatic design. *2D Mater.* **2018**, *5*, 035019. [[CrossRef](#)]
24. Liao, F.; Guo, Z.; Wang, Y.; Xie, Y.; Zhang, S.; Sheng, Y.; Tang, H.; Xu, Z.; Riaud, A.; Zhou, P.; et al. High-Performance Logic and Memory Devices Based on a Dual-Gated MoS₂ Architecture. *ACS Appl. Electron. Mater.* **2019**, *2*, 111–119. [[CrossRef](#)]
25. Yu, S.H.; Lee, Y.B.; Jang, S.K.; Kang, J.; Jeon, J.; Lee, C.G.; Lee, J.Y.; Kim, H.; Hwang, E.; Lee, S.; et al. Dye-Sensitized MoS₂ Photodetector with Enhanced Spectral Photoresponse. *ACS Nano* **2014**, *8*, 8285–8291. [[CrossRef](#)]
26. Gan, L.-Y.; Zhang, Q.; Cheng, Y.; Schwingschlögl, U. Photovoltaic Heterojunctions of Fullerenes with MoS₂ and WS₂ Monolayers. *J. Phys. Chem. Lett.* **2014**, *5*, 1445–1449. [[CrossRef](#)]
27. Kuru, C.; Choi, C.; Kargar, A.; Choi, D.; Kim, Y.J.; Liu, C.H.; Yavuz, S.; Jin, S. MoS₂ Nanosheet-Pd Nanoparticle Composite for Highly Sensitive Room Temperature Detection of Hydrogen. *Adv. Sci.* **2015**, *2*, 1500004. [[CrossRef](#)]
28. Tabata, H.; Matsuyama, H.; Goto, T.; Kubo, O.; Katayama, M. Visible-Light-Activated Response Originating from Carrier-Mobility Modulation of NO₂ Gas Sensors Based on MoS₂ Monolayers. *ACS Nano* **2021**, *15*, 2542–2553. [[CrossRef](#)]
29. Bai, J.; Shen, Y.; Zhao, S.; Chen, Y.; Li, G.; Han, C.; Wei, D.; Yuan, Z.; Meng, F. Flower-like MoS₂ hierarchical architectures assembled by 2D nanosheets sensitized with SnO₂ quantum dots for high-performance NH₃ sensing at room temperature. *Sens. Actuators B Chem.* **2021**, *353*, 131191. [[CrossRef](#)]
30. Hou, S.; Pang, R.; Chang, S.; Ye, L.; Xu, J.; Wang, X.-C.; Zhang, Y.; Shang, Y.; Cao, A. Synergistic CNFs/CoS₂/MoS₂ Flexible Films with Unprecedented Selectivity for NO Gas at Room Temperature. *ACS Appl. Mater. Interfaces* **2020**, *12*, 29778–29786. [[CrossRef](#)]

31. Lee, K.; Gatensby, R.; McEvoy, N.; Hallam, T.; Duesberg, G.S. High-Performance Sensors Based on Molybdenum Disulfide Thin Films. *Adv. Mater.* **2013**, *25*, 6699–6702. [[CrossRef](#)] [[PubMed](#)]
32. Liu, B.; Chen, L.; Liu, G.; Abbas, A.N.; Fathi, M.; Zhou, C. High-Performance Chemical Sensing Using Schottky-Contacted Chemical Vapor Deposition Grown Monolayer MoS₂ Transistors. *ACS Nano* **2014**, *8*, 5304–5314. [[CrossRef](#)] [[PubMed](#)]
33. Li, H.; Yin, Z.; He, Q.; Li, H.; Huang, X.; Lu, G.; Fam, D.W.H.; Tok, A.I.Y.; Zhang, Q.; Zhang, H. Fabrication of Single- and Multilayer MoS₂ Film-Based Field-Effect Transistors for Sensing NO at Room Temperature. *Small* **2011**, *8*, 63–67. [[CrossRef](#)]
34. Zhou, Q.; Hong, C.; Yao, Y.; Hussain, S.; Xu, L.; Zhang, Q.; Gui, Y.; Wang, M. Hierarchically MoS₂ nanospheres assembled from nanosheets for superior CO gas-sensing properties. *Mater. Res. Bull.* **2018**, *101*, 132–139. [[CrossRef](#)]
35. Ozaki, F.; Tanaka, S.; Osada, W.; Mukai, K.; Horio, M.; Koitaya, T.; Yamamoto, S.; Matsuda, I.; Yoshinobu, J. Functionalization of the MoS₂ basal plane for activation of molecular hydrogen by Pd deposition. *Appl. Surf. Sci.* **2022**, *593*. [[CrossRef](#)]
36. Alagh, A.; Annanouch, F.E.; Umek, P.; Bittencourt, C.; Colomer, J.F.; Llobet, E. An Ultrasensitive Room-Temperature H₂S Gas Sensor Based on 3D Assembly of Cu₂O Decorated WS₂ Nanomaterial. *IEEE Sens. J.* **2021**, *21*, 21212–21220. [[CrossRef](#)]
37. Annanouch, F.E.; Haddi, Z.; Ling, M.; di Maggio, F.; Vallejos, S.; Vilic, T.T.; Zhu, Y.; Shujah, T.; Umek, P.; Bittencourt, C.; et al. Aerosol-Assisted CVD-Grown PdO Nanoparticle-Decorated Tungsten Oxide Nanoneedles Extremely Sensitive and Selective to Hydrogen. *ACS Appl. Mater. Interfaces* **2016**, *8*, 10413–10421. [[CrossRef](#)]
38. Baek, D.-H.; Kim, J. MoS₂ gas sensor functionalized by Pd for the detection of hydrogen. *Sens. Actuators B Chem.* **2017**, *250*, 686–691. [[CrossRef](#)]
39. Gottam, S.R.; Tsai, C.-T.; Wang, L.-W.; Wang, C.-T.; Lin, C.-C.; Chu, S.-Y. Highly sensitive hydrogen gas sensor based on a MoS₂-Pt nanoparticle composite. *Appl. Surf. Sci.* **2019**, *506*, 144981. [[CrossRef](#)]
40. Urs, K.M.B.; Katiyar, N.K.; Kumar, R.; Biswas, K.; Singh, A.K.; Tiwary, C.S.; Kamble, V. Multi-component (Ag–Au–Cu–Pd–Pt) alloy nanoparticle-decorated p-type 2D-molybdenum disulfide (MoS₂) for enhanced hydrogen sensing. *Nanoscale* **2020**, *12*, 11830–11841. [[CrossRef](#)]
41. Lee, J.-H.; Mirzaei, A.; Kim, J.-Y.; Kim, J.-H.; Kim, H.W.; Kim, S.S. Optimization of the surface coverage of metal nanoparticles on nanowires gas sensors to achieve the optimal sensing performance. *Sens. Actuators B Chem.* **2019**, *302*, 127196. [[CrossRef](#)]
42. Lee, J.-S.; Katoch, A.; Kim, J.-H.; Kim, S.S. Effect of Au nanoparticle size on the gas-sensing performance of p-CuO nanowires. *Sens. Actuators B Chem.* **2016**, *222*, 307–314. [[CrossRef](#)]
43. Kim, S.S.; Park, J.Y.; Choi, S.-W.; Kim, H.S.; Gil Na, H.; Yang, J.C.; Lee, C.; Kim, H.W. Room temperature sensing properties of networked GaN nanowire sensors to hydrogen enhanced by the Ga₂Pd₅ nanodot functionalization. *Int. J. Hydrog. Energy* **2011**, *36*, 2313–2319. [[CrossRef](#)]
44. Stolze, M.; Gogova, D.; Thomas, L.-K. Analogy for the maximum obtainable colouration between electrochromic, gasochromic, and electrocolouration in DC-sputtered thin WO_{3–y} films. *Thin Solid Films* **2005**, *476*, 185–189. [[CrossRef](#)]
45. Hwang, I.-S.; Choi, J.-K.; Woo, H.-S.; Kim, S.-J.; Jung, S.-Y.; Seong, T.-Y.; Kim, I.-D.; Lee, J.-H. Facile Control of C₂H₅OH Sensing Characteristics by Decorating Discrete Ag Nanoclusters on SnO₂ Nanowire Networks. *ACS Appl. Mater. Interfaces* **2011**, *3*, 3140–3145. [[CrossRef](#)] [[PubMed](#)]
46. Late, D.J.; Huang, Y.-K.; Liu, B.; Acharya, J.; Shirodkar, S.N.; Luo, J.; Yan, A.; Charles, D.; Waghmare, U.V.; Dravid, V.P.; et al. Sensing Behavior of Atomically Thin-Layered MoS₂ Transistors. *ACS Nano* **2013**, *7*, 4879–4891. [[CrossRef](#)]
47. Eom, T.H.; Cho, S.H.; Suh, J.M.; Kim, T.; Lee, T.H.; Jun, S.E.; Yang, J.W.; Lee, J.; Hong, S.-H.; Jang, H.W. Substantially improved room temperature NO₂ sensing in 2-dimensional SnS₂ nanoflowers enabled by visible light illumination. *J. Mater. Chem. A* **2021**, *9*, 11168–11178. [[CrossRef](#)]
48. Park, J.; Mun, J.; Shin, J.-S.; Kang, S.-W. Highly sensitive two-dimensional MoS₂ gas sensor decorated with Pt nanoparticles. *R. Soc. Open Sci.* **2018**, *5*, 181462. [[CrossRef](#)]
49. Suh, J.M.; Shim, Y.-S.; Kwon, K.C.; Jeon, J.-M.; Lee, T.H.; Shokouhimehr, M.; Jang, H.W. Pd- and Au-Decorated MoS₂ Gas Sensors for Enhanced Selectivity. *Electron. Mater. Lett.* **2019**, *15*, 368–376. [[CrossRef](#)]
50. Burman, D.; Raha, H.; Manna, B.; Pramanik, P.; Guha, P.K. Substitutional Doping of MoS₂ for Superior Gas-Sensing Applications: A Proof of Concept. *ACS Sens.* **2021**, *6*, 3398–3408. [[CrossRef](#)]
51. Huang, X.; Zeng, Z.; Bao, S.; Wang, M.; Qi, X.; Fan, Z.; Zhang, H. Solution-phase epitaxial growth of noble metal nanostructures on dispersible single-layer molybdenum disulfide nanosheets. *Nat. Commun.* **2013**, *4*, 1444. [[CrossRef](#)] [[PubMed](#)]
52. Kim, T.; Lee, T.H.; Park, S.Y.; Eom, T.H.; Cho, I.; Kim, Y.; Kim, C.; A Lee, S.; Choi, M.-J.; Suh, J.M.; et al. Drastic Gas Sensing Selectivity in 2-Dimensional MoS₂ Nanoflakes by Noble Metal Decoration. *ACS Nano* **2023**, *17*, 4404–4413. [[CrossRef](#)] [[PubMed](#)]
53. Lee, S.; Kang, Y.; Lee, J.; Kim, J.; Shin, J.W.; Sim, S.; Go, D.; Jo, E.; Kye, S.; Kim, J.; et al. Atomic layer deposited Pt nanoparticles on functionalized MoS₂ as highly sensitive H₂ sensor. *Appl. Surf. Sci.* **2021**, *571*, 151256. [[CrossRef](#)]
54. Alagh, A.; Annanouch, F.E.; Al Youssef, K.; Bittencourt, C.; Güell, F.; Martínez-Alanis, P.R.; Reguant, M.; Llobet, E. PdO and PtO loaded WS₂ boosts NO₂ gas sensing characteristics at room temperature. *Sens. Actuators B Chem.* **2022**, *364*. [[CrossRef](#)]
55. Alagh, A.; Annanouch, F.E.; Umek, P.; Bittencourt, C.; Sierra-Castillo, A.; Haye, E.; Colomer, J.F.; Llobet, E. CVD growth of self-assembled 2D and 1D WS₂ nanomaterials for the ultrasensitive detection of NO₂. *Sens. Actuators B Chem.* **2020**, *326*, 128813. [[CrossRef](#)]
56. Li, S.; Wang, S.; Salamone, M.M.; Robertson, A.W.; Nayak, S.; Kim, H.; Tsang, S.C.E.; Pasta, M.; Warner, J.H. Edge-Enriched 2D MoS₂ Thin Films Grown by Chemical Vapor Deposition for Enhanced Catalytic Performance. *ACS Catal.* **2016**, *7*, 877–886. [[CrossRef](#)]

57. Shomalian, K.; Bagheri-Mohagheghi, M.-M.; Ardyanian, M. Characterization and study of reduction and sulfurization processing in phase transition from molybdenum oxide (MoO₂) to molybdenum disulfide (MoS₂) chalcogenide semiconductor nanoparticles prepared by one-stage chemical reduction method. *Appl. Phys. A* **2016**, *123*, 93. [[CrossRef](#)]
58. Ramakrishnan, V.; Alex, C.; Nair, A.N.; John, N.S. Designing Metallic MoO₂ Nanostructures on Rigid Substrates for Electrochemical Water Activation. *Chem.–A Eur. J.* **2018**, *24*, 18003–18011. [[CrossRef](#)]
59. Lee, C.; Yan, H.; Brus, L.E.; Heinz, T.F.; Hone, J.; Ryu, S. Anomalous Lattice Vibrations of Single- and Few-Layer MoS₂. *ACS Nano* **2010**, *4*, 2695–2700. [[CrossRef](#)]
60. Annanouch, F.E.; Alagh, A.; Umek, P.; Casanova-Chafer, J.; Bittencourt, C.; Llobet, E. Controlled growth of 3D assemblies of edge enriched multilayer MoS₂ nanosheets for dually selective NH₃ and NO₂ gas sensors. *J. Mater. Chem. C* **2022**, *10*, 11027–11039. [[CrossRef](#)]
61. Bendahan, M.; Guérin, J.; Boulmani, R.; Aguir, K. WO₃ sensor response according to operating temperature: Experiment and modeling. *Sens. Actuators B Chem.* **2007**, *124*, 24–29. [[CrossRef](#)]
62. Park, S.; Garcia-Esparza, A.T.; Abroshan, H.; Abraham, B.; Vinson, J.; Gallo, A.; Nordlund, D.; Park, J.; Kim, T.R.; Vallez, L.; et al. Operando Study of Thermal Oxidation of Monolayer MoS₂. *Adv. Sci.* **2021**, *8*, 2002768. [[CrossRef](#)] [[PubMed](#)]
63. Park, C.H.; Koo, W.-T.; Lee, Y.J.; Kim, Y.H.; Lee, J.; Jang, J.-S.; Yun, H.; Kim, I.-D.; Kim, B.J. Hydrogen Sensors Based on MoS₂ Hollow Architectures Assembled by Pickering Emulsion. *ACS Nano* **2020**, *14*, 9652–9661. [[CrossRef](#)] [[PubMed](#)]
64. Kowalska, E.; Czerwosz, E.; Diduszko, R.; Kaminska, A.; Danila, M. Influence of PdHx formation ability on hydrogen sensing properties of palladium-carbonaceous films. *Sens. Actuators A Phys.* **2013**, *203*, 434–440. [[CrossRef](#)]
65. Huang, Z.; Luo, W.; Ma, L.; Yu, M.; Ren, X.; He, M.; Polen, S.; Click, K.; Garrett, B.; Lu, J.; et al. Dimeric [Mo₂S₁₂]²⁻ Cluster: A Molecular Analogue of MoS₂ Edges for Superior Hydrogen-Evolution Electrocatalysis. *Angew. Chem. Int. Ed.* **2015**, *54*, 15181–15185. [[CrossRef](#)]
66. Tang, X.; Haddad, P.-A.; Mager, N.; Geng, X.; Reckinger, N.; Hermans, S.; Debliquy, M.; Raskin, J.-P. Chemically deposited palladium nanoparticles on graphene for hydrogen sensor applications. *Sci. Rep.* **2019**, *9*, 1–11. [[CrossRef](#)]
67. Jaiswal, J.; Tiwari, P.; Singh, P.; Chandra, R. Fabrication of highly responsive room temperature H₂ sensor based on vertically aligned edge-oriented MoS₂ nanostructured thin film functionalized by Pd nanoparticles. *Sens. Actuators B Chem.* **2020**, *325*. [[CrossRef](#)]
68. Matsunaga, N.; Sakai, G.; Shimano, K.; Yamazoe, N. Diffusion equation-based study of thin film semiconductor gas sensor-response transient. *Sens. Actuators B Chem.* **2002**, *83*, 216–221. [[CrossRef](#)]
69. Matsunaga, N.; Sakai, G.; Shimano, K.; Yamazoe, N. Formulation of gas diffusion dynamics for thin film semiconductor gas sensor based on simple reaction–diffusion equation. *Sens. Actuators B Chem.* **2003**, *96*, 226–233. [[CrossRef](#)]
70. Suresh, S.; Urs, K.M.B.; Vasudevan, A.T.; Sriram, S.; Kamble, V.B. Analysis of Unusual and Instantaneous Overshoot of Response Transients in Gas Sensors. *Phys. Status Solidi (RRL)–Rapid Res. Lett.* **2019**, *13*. [[CrossRef](#)]
71. Darmadi, I.; Nugroho, F.A.A.; Langhammer, C. High-Performance Nanostructured Palladium-Based Hydrogen Sensors—Current Limitations and Strategies for Their Mitigation. *ACS Sens.* **2020**, *5*, 3306–3327. [[CrossRef](#)]
72. Wang, J.; Yang, Y.; Xia, Y. Mesoporous MXene/ZnO nanorod hybrids of high surface area for UV-activated NO₂ gas sensing in ppb-level. *Sens. Actuators B Chem.* **2022**, *353*. [[CrossRef](#)]
73. Rsan, N.B.; Weimar, U. Understanding the fundamental principles of metal oxide based gas sensors; the example of CO sensing with SnO₂ sensors in the presence of humidity. *J. Phys. Condens. Matter* **2003**, *15*, R813–R839. [[CrossRef](#)]
74. Hashtroudi, H.; Atkin, P.; Mackinnon, I.D.R.; Shafiei, M. Low-operating temperature resistive nanostructured hydrogen sensors. *Int. J. Hydrog. Energy* **2019**, *44*, 26646–26664. [[CrossRef](#)]
75. Mirzaei, A.; Yousefi, H.R.; Falsafi, F.; Bonyani, M.; Lee, J.-H.; Kim, J.-H.; Kim, H.W.; Kim, S.S. An overview on how Pd on resistive-based nanomaterial gas sensors can enhance response toward hydrogen gas. *Int. J. Hydrog. Energy* **2019**, *44*, 20552–20571. [[CrossRef](#)]
76. Chacko, L.; Massera, E.; Aneesh, P.M. Enhancement in the Selectivity and Sensitivity of Ni and Pd Functionalized MoS₂ Toxic Gas Sensors. *J. Electrochem. Soc.* **2020**, *167*, 106506. [[CrossRef](#)]
77. Asakuma, Y.; Miyauchi, S.; Yamamoto, T.; Aoki, H.; Miura, T. Numerical analysis of absorbing and desorbing mechanism for the metal hydride by homogenization method. *Int. J. Hydrog. Energy* **2003**, *28*, 529–536. [[CrossRef](#)]

Disclaimer/Publisher’s Note: The statements, opinions and data contained in all publications are solely those of the individual author(s) and contributor(s) and not of MDPI and/or the editor(s). MDPI and/or the editor(s) disclaim responsibility for any injury to people or property resulting from any ideas, methods, instructions or products referred to in the content.